Chapter 5

Magnetic and Dielectric properties of $BaFe_{12-x}Ni_xO_{19}$, BHNF (x = 0.0,0.05,0.1,and 0.2) ceramic synthesized by Chemical route

5.1. Introduction

Barium hexaferrite with chemical composition, $MFe_{12}O_{19}$ (M= Ba, Sr or Pb) having considerable attention in electronic applications such as permanent magnet, high-density magnetic recording media, microwave device and telecommunications equipment. These important applications of this material are due to strong uniaxial crystalline anisotropy, high saturated magnetic polarization, large coercivity and high resonant frequency with an excellent capability and corrosion resistance [Singhal *et al.* (2011), Onreabroy *et al.* (2012), Zhang *et al.* (2007)]. The large crystal anisotropy and high intrinsic coercivity of this material is responsible for high stability and electrical resistivity. The hexaferrite ($BaFe_{12}O_{19}$) have M-type structure which exhibits strong ferromagnetism among ferrites. It has widely used in electronic device and their properties strongly depend on microstructure and morphology. These materials have high relevance in higher frequency, high resistance to the heat and corrosion than others due to high coercivity with small particle size [Pereira *et al.* (2009)]. The magnetic and dielectric properties of ferrites have been strongly influenced by synthesis procedures and substitution of various cations such as divalent and trivalent [Ahamed *et al.* (2004)]. The various synthesis methods for the fabrication of M-type hexaferrite ceramic has been used, such as ceramic method [Almeida *et al.* (2009)], citrate auto-combustion synthesis [Shirtcliffe *et al.* (2007)], co-precipitation [Ahmed *et al.* (2015)], mechano-thermal treatment [Molaeia *et al.* (2012)], sol-gel , microemulsion techniques [Jotania *et al.* (2008)], ball milling [Molaei *et al.* (2012)], wet mixing method [Song *et al.* (2014)] and hydrothermal [Chang *et al.* (2012)]. The substitution of divalent and tetravalent (Co^{+2}, Ni^{+2}, Ti^{+4}) cations at the site of Fe^{+3} and Ba have been carried out for the improvement of magnetic properties [Haijun *et al.* (2003), Li *et al.* (2000)]. These improvements have occurred

because of their similarity in ionic radii and their electronic configuration. Their magnetic properties may be conjointly enhance by the substitution of Fe^{+3} with magnetic or non-magnetic ions which results in significant change in saturation magnetization because of modification within the net magnetic moment per molecules [Mahmood *et al.* (2015), Cao *et al.* (2014), Lu *et al.* (2014), Pan (2014)]. The substitution of Mn^{+3}, La^{+3}, Co^{+2}-Zr^{+4}, Ti^{+4}-Mn^{+4}, Co^{+2}-Ti^{+4} ions have been decreased in saturation magnetization (Ms) and coercivity (Hc) [Iqbal and Farooq (2010)]. This decrease is due to presence of secondary phase which also inhibits the recording application of material. Most of the works have been carried out for the synthesis and characterization of M-type barium hexaferrite, for examples $BaFe_{12}O_{19}$, $BaMe_xFe_{12-x}O_{19}$ (Me^{+3} = Al, Cr, Bi, Sc), $BaMe_xIr_xFe_{12-2x}O_{19}$ (Me^{+2} = Co, Zn), $BaZn_xSn_xFe_{12-2x}O_{19}$, $BaCo_xRu_xFe_{12-2x}O_{19}$, $BaMe_xTi_xFe_{11.6-2x}O_{19}$ (Me^{+2} = Co, Zn), and $BaMe_xTi_xFe_{12-2x}O_{19}$ (Me^{+2} = Co, Zn, Mn) etc. [Zhao *et al.* (2005)].

In the present study, we studied the effect of Ni^{+2} substitutions for the improvement of electrical and magnetic properties of $BaFe_{12}O_{19}$ ceramic synthesized by chemical route. The chemical route is more suitable than other synthesis methods for the preparation of nanostructure materials. It was observed that substituting Fe^{+3} by Ni^{+2} ions reduces coercivity and saturation magnetization which is a major factor for recording data [Rane *et al.* (1999)].

5.2. Experimental

5.2.1. Material Synthesis

Nickel doped barium hexaferrite was synthesized by the chemical route using analytical grade chemicals, Ba $(NO_3)_2$ (99% Merck, India), Fe $(NO_3)_3$.$9H_2O$ (98% Merck, India) and Ni $(NO_3)_2$ (99% Merck, India) as starting materials. The stoichiometric amount of metal nitrates was dissolved in de-ionized distilled water along with appropriate amount of citric acid ($C_6H_8O_7$

.H_2O, 99% Merck, India) as per equivalent to the metal ions. The resulting solution was heated on a hot plate with magnetic stirrer at 70 – 80 °C to evaporate excesses water. On further heating, a fluffy mass was obtained which burns with a sooty flame. The obtained porous ash was crushed into fine powder with the help of mortar and pestle. The resultant dry powder was calcined at 800 °C for 8 h in the electrical muffle furnace after that cylindrical pellets (13.0 mm diameters, 1.6 mm thicknesses) was prepared using 2 wt% polyvinyl alcohol (PVA) as a binder. These pellets were sintered at 1200 °C for 6 h and further used for different physiochemical characterizations such as XRD, SEM, TEM, EDX, and AFM.

5.2.2. Characterization

The crystalline phase of sintered BHNF ceramic was identified by X-ray diffraction analysis (Rigakuminiflex 600, Japan) employing Cu-Kα radiation (λ = 1.54 Å). The microstructure and elemental analysis of the BHNF ceramic were observed by scanning electron microscope (ZEISS, model EVO–18 research; Germany), energy-dispersive X-ray spectroscopy (EDX, Oxford instrument; USA), respectively. Transmission electron microscope (TEM, FEI TECANI G^2 20 TWIN; USA) was used for particle size determination. The surface morphology was examined by atomic force microscopy (NTEGRA Prima, Germany). The ferroelectric properties of the sintered BHNF ceramic were measured by ferroelectric tracer (Automatic P-E loop tracer, Marin India). Magnetic behavior and temperature dependence Zero Field Cooled (M^{ZFC}), Field Cooled (M^{FC}) over a temperature range 5 – 300 K and applied a magnetic field 2 tesla (± 2 T) were recorded by Quantum Design MPMS-3 and SQUID VSM dc magnetometer respectively. The frequency and temperature dependence dielectric of silver coated pellets were carried out using LCR meter (PSM 1735, NumetriQ 4^{th} Ltd. U.K.).

5.3. Results and discussion

5.3.1. Crystallinity and Microstructural Studies

XRD patterns of BHNF ceramic sintered at 1200 °C for 6 h is shown in Figure 5.1. The single phase formation of the hexagonal BHNF ceramic with the composition x= 0.0, 0.05, 0.1 and 0.2 is confirmed with JCPDS card no. (78–0132). The average crystallite size is calculated by the Debye Scherer formula [Singh *et al.* (2011)].

$$D = k\lambda/\beta \cos\theta \tag{5.1}$$

where, D is the crystallite size, k is a constant value taken as 0.96, λ is the wavelength of X–ray, θ is the Bragg angle of peaks, and β represents full width at half maxima (FWHM).

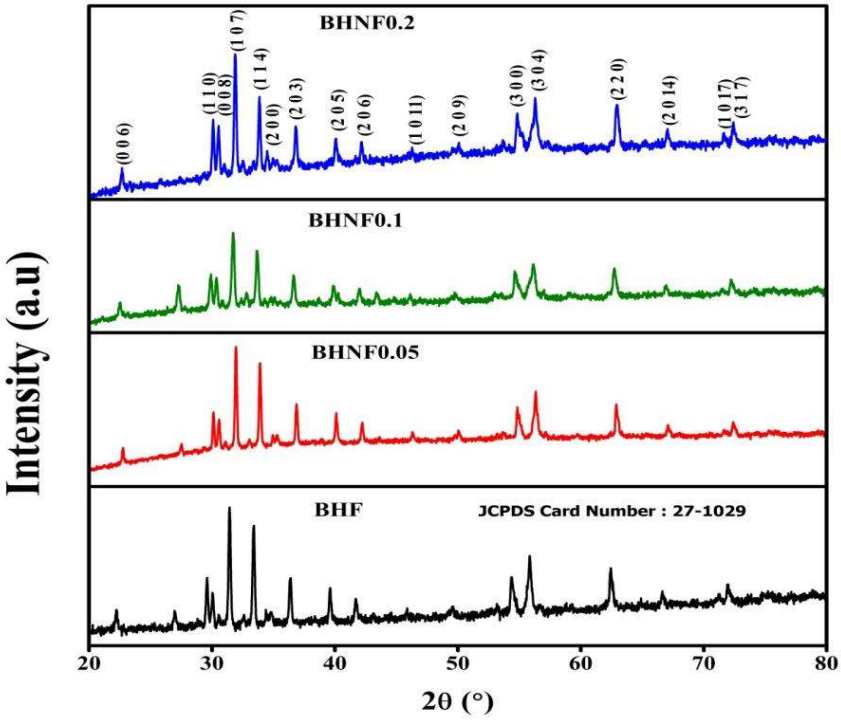

Figure 5.1 Shows XRD diffraction patterns of $BaFe_{12-x}Ni_xO_{19}$ (x= 0.0, 0.05, 0.1, and 0.2) ceramic a sintered at 1200 °C for 6 h.

The average crystallite size of BHNF ceramic is found to be 51.12, 50.13, 48.90, and 30.71 nm for x = 0.0, 0.05, 0.1 and 0.2, respectively.

Le-Bail full pattern matching analysis is also performing for phase determination of BHNF ceramic, shown in Figure 5.2. The overlapping of the calculated pattern indicated by red color and observed pattern assigned by black color are sustaining the good fitting of the XRD patterns. The difference between observed and calculated pattern plotted above the bottom line is assigned by the vertical tick mark (green color) are good agreement with the lower value of χ^2, indicating the goodness of fitting of the XRD pattern.

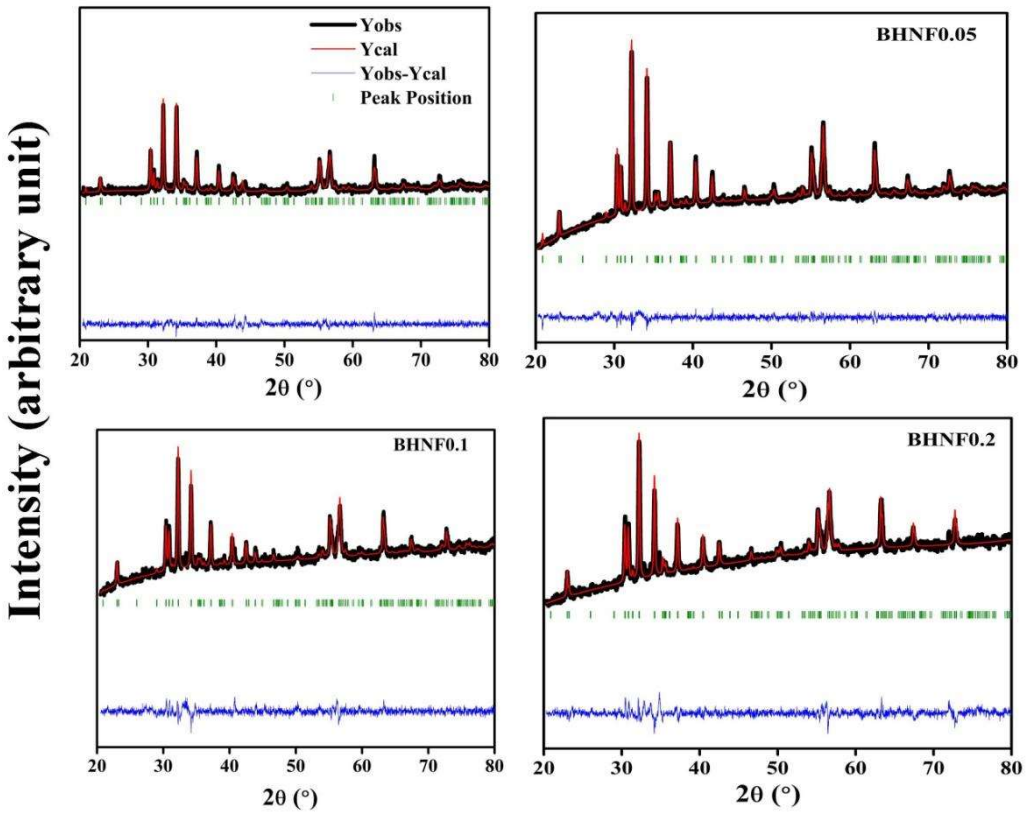

Figure 5.2 Le-Bail full pattern matching analysis of XRD patterns for $BaFe_{12-x}Ni_xO_{19}$ (BHFC) ceramic with compositions x= 0.0, 0.05, 0.1, and 0.2 sintered at 1200 °C for 6 h.

All the observed Bragg's peaks confirm the space group $P6_3/mmc$ of the BHNF ceramic i.e., hexagonal structure [Pratap Behera and S. Ravi (2017)]. The refined value of lattice parameter, angles, Bragg R-factor and RF-factor for all the compositions of BHNF ceramic is also listed in table 5.1.

Table 5.1 Lattice parameters, crystal structures, angles, Bragg R-factor and RF-factor for $BaFe_{12-x}Ni_xO_{19}$ (x = 0.0, 0.05, 0.1, 0.2) Ceramic.

Phase: $BaFe_{12}O_{19}$, Space group: $P6_3/mmc$, Angle: $\alpha = \beta = 90°$, $\gamma = 120°$, Hexagonal

Samples			Lattice parameters (Å)		Bragg R-factor	RF-factor
$BaFe_{12-x}Ni_xO_{19}$	χ^2	Crystallize size (nm)	a = b	c		
X = 0.0	1.17	51.12	5.884550	23.182034	2.145	2.197
X = 0.05	1.80	50.13	5.886025	23.211716	5.910	6.075
X = 0.1	1.70	48.90	5.877505	23.164640	2.874	3.092
X= 0.2	1.84	30.71	5.878628	23.185991	3.904	4.318

To understand the functional group of BHNF ceramic, FTIR spectrum recorded in the frequency range 400 – 4000 cm^{-1} are shown in Figure 5.3. There are two absorption peaks observed in the frequency range in between 500 and 800 cm^{-1} which is associated with Fe–O stretching vibration bands due to octahedral and tetrahedral sites [Rostami *et al.* (2016)]. The peaks of metal-oxygen bonds appeared at 895 cm^{-1} are corresponding to the bonding in between barium and oxygen atom (Ba-O).The existence of the broad absorption band at 1630 as well as 3440 cm^{-1} are due to

hydroxyl (OH) functional group and moist atmosphere. The absorption peaks are attributable to metal-oxygen–metal bonds such as Fe–O–Fe bonds, are also found in the frequency ranges 1100-1500 cm^{-1}. The observed absorption peaks confirm the formation of hexaferrite [Ahmed *et al.* (2015)].

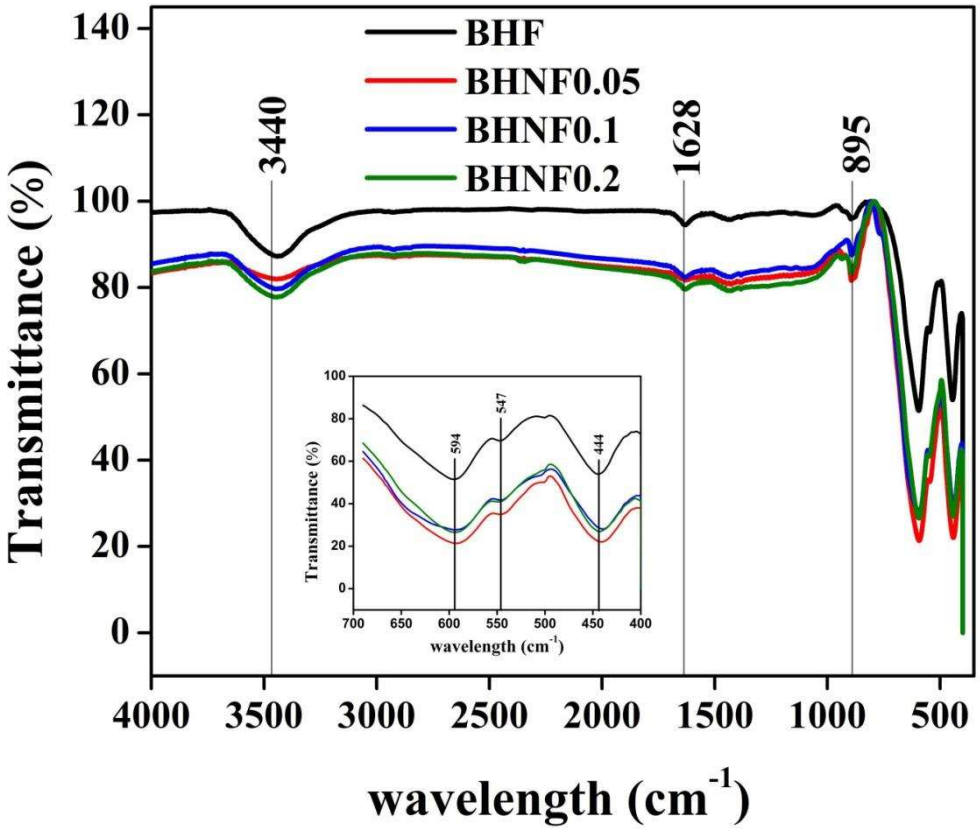

Figure 5.3 FTIR spectra of $BaFe_{12-x}Ni_xO_{19}$ (BHFC) ceramic with compositions x= 0.0, 0.05, 0.1, and 0.2 ceramic sintered at 1200 °C for 6 h

The bright field TEM images of BHNF ceramic sintered at 1200 °C for 6 h is shown in Figure 5.4a, a′, a″, and a‴ which reveals the presence of hexagonal shape particles of size 332, 221, and 120 nm on the scale 200 nm for the composition x = 0.0, 0.05 and 0.1, however particle size of BHNF ceramic with composition x = 0.2 obtained by image J software was found to be

16 nm measured on the scale 50 nm. It is revealed that particle size of the BHNF ceramic were decreases with increasing Ni concentration. With the help of selected area diffraction (SAED) patterns mentioned in the Figure 5.4b, b′, b″, and b‴, it is observed that various diffraction for different composition passes through the different planes. The zone axis containing [(2 2 0), (1 0 11)], [(1 0 6), (0 0 6)], [(1 1 4), (1 1 0)] and [(2 0 0), (1 0 2)] planes are calculated to be [22 $\overline{22}$ $\overline{2}$], [0 6 0], [$\overline{4}$ $\overline{4}$ 0] and [0 4 0] for the composition x= 0.0, 0.05, 0.1 and 0.2, respectively.

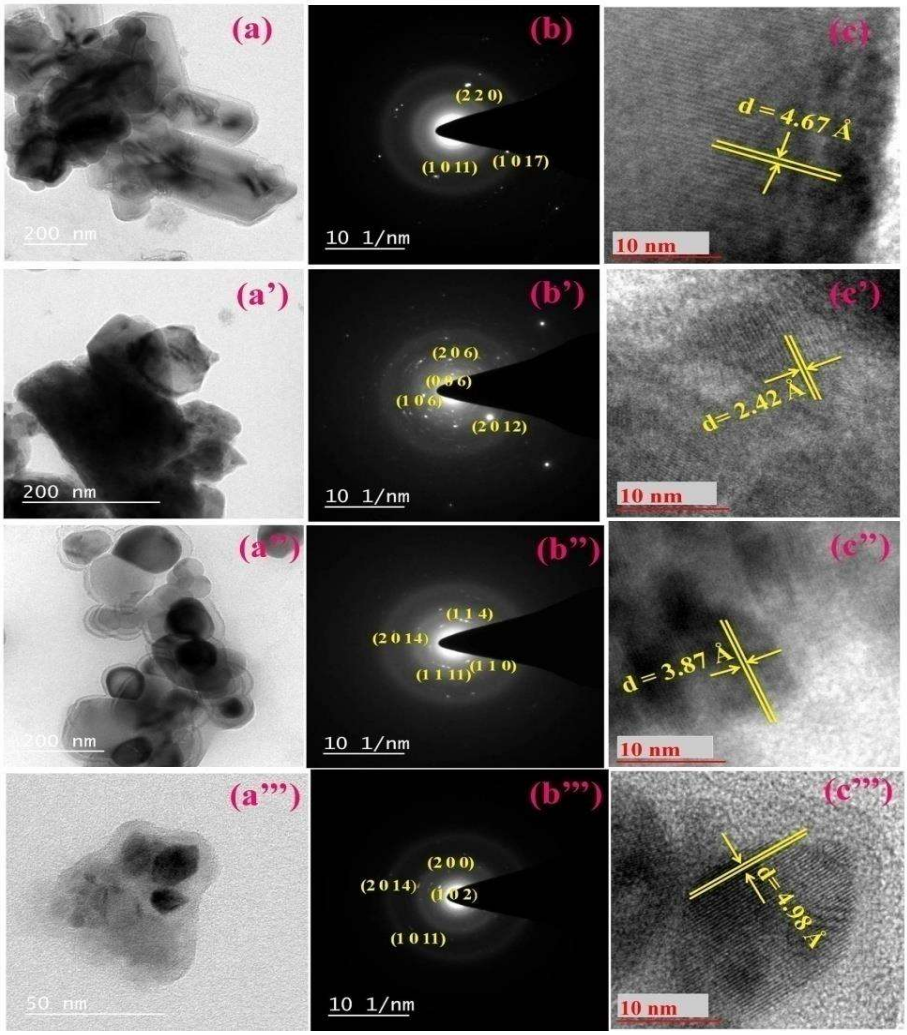

Figure 5.4 (a, a′, a″, a‴)Bright field TEM image (b, b′, b″, b‴) selected area diffraction (SAED) pattern (c, c′, c″, c‴) High-resolution TEM image of BHNF ceramic sintered 1200 °C for 6 h.

Figure 5.4c, c′, c″, and c‴ show the high resolution (HR–TEM) image showing the corresponding planes (1 0 2), (2 0 3), (0 0 6) and (1 0 1) having d-spacing 0.467, 0.242, 0.387 and 0.498 nm, respectively. All the indexed planes obtained by HR-TEM and SAED pattern are in good agreement with XRD results which confirmed the hexagonal nature of the material.

Figure 5.5a-d shows hexagonal plate-like grains which are separated by well-defined grain boundaries. The average grain size obtained by Image J software is found to be 339, 436, 456, 496 nm for the composition x = 0.0, 0.05, 0.1 and 0.2, respectively which indicates that the average grain of BHNF ceramic increases with increasing the concentration of Ni ion.

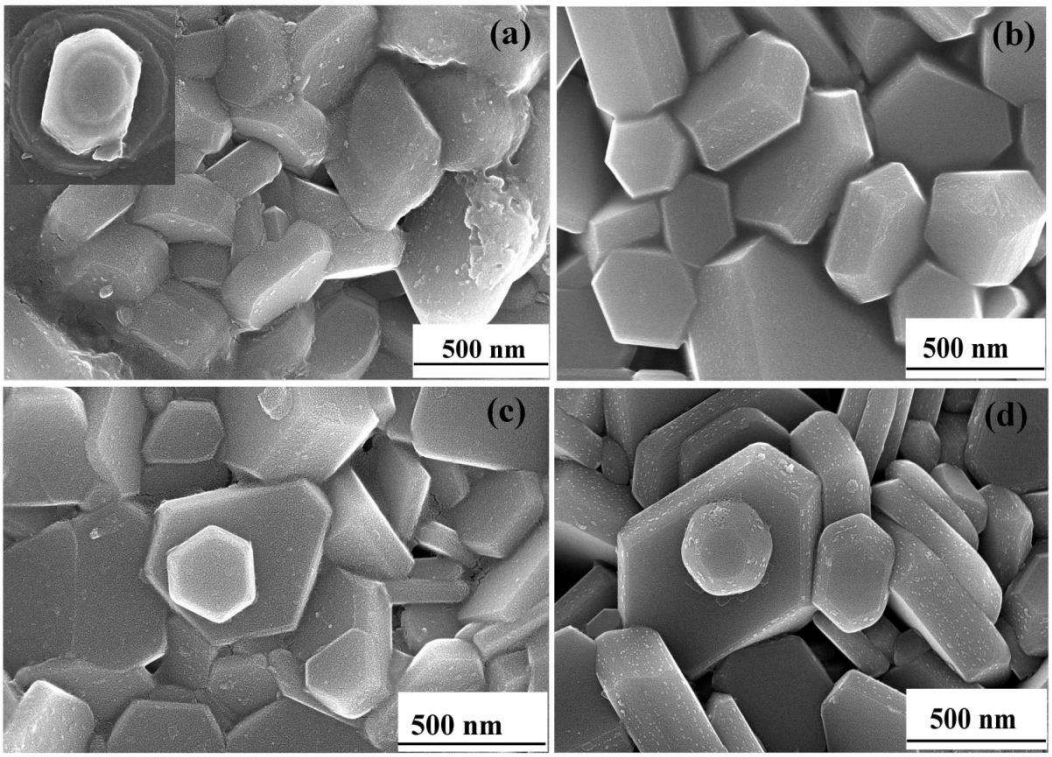

Figure 5.5 a, b, c and d indicate SEM image of BHNF ceramic with compositions x = 0.0, 0.05, 0.1, and 0.2 sintered at 1200 °C for 6 h.

Furthermore, the average grain size of BHNF ceramic observed from the SEM analysis is larger than crystallite as well as particle size due to crystallites are formed by combination of few

particles whereas grains by agglomeration. The pH of the solution also affected on the morphology of the particles of the barium hexaferrite as a result of which particle size will increase with the decrease of pH which can ensure to decrease within the rate of growth or increasing the nucleation rate of the particles.

The EDX spectra of BHNF ceramic indicates the presence of Ba, Fe, Ni and O elements as shown in Figure 5.6a. The atomic percentages of Ba, Fe, Ni and O are found to be 3.96, 42.90, 1.13 and 52.01, respectively and weight percentage 14.18, 62.41, 1.72 and 21.68, respectively that confirm the purity of the materials. Figure 5.6b–d shows energy dispersive mapping which indicates the homogeneous distribution of the corresponding elements in BHNF ceramic.

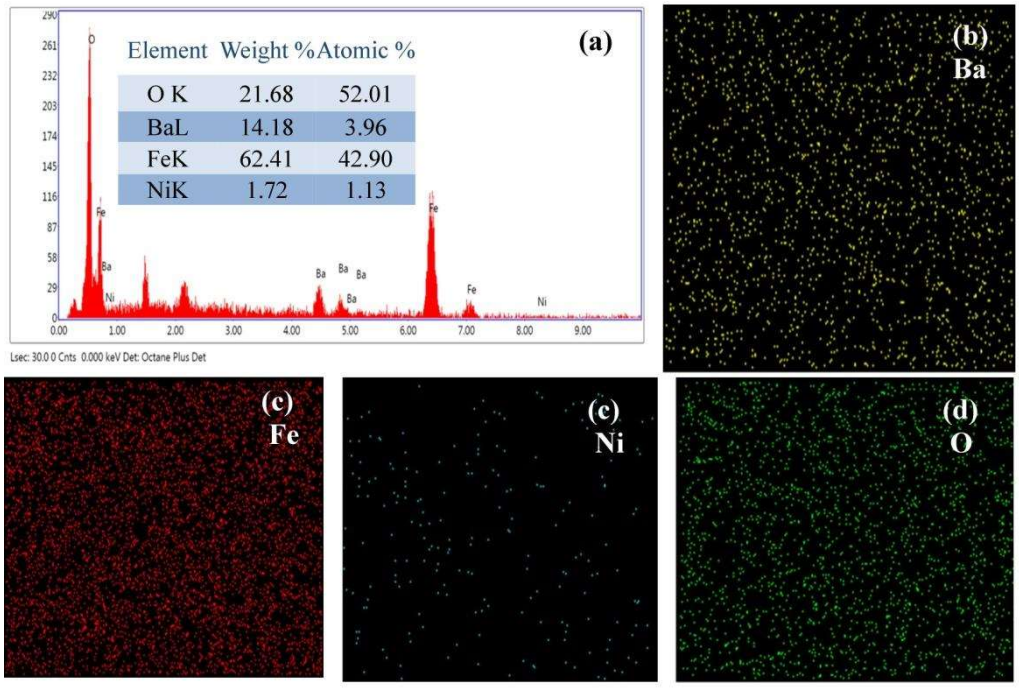

Figure 5.6 (a) EDX spectra (b) EDX mapping of BHNF ceramic sintered at sintered 1200 °C for 6 h.

Figure 5.7a represents the two-dimensional AFM image of BHNF ceramic with composition x = 0.2 sintered at 1200 °C for 6 h, the surface morphology reveals the homogenous

distribution of grains are separated by grain boundaries. The three-dimensional image of BNHF ceramic is shown in Figure 5.7b**,** after thorough analysis of the grains, we observed the average roughness (R_a), root mean square roughness (R_q), maximum area peak height (Sp) and maximum peak-valley depth are 53 nm, 68 nm, 255 nm and 287 nm, respectively. Figure 5.7c shows the histogram of grain size which indicates that the majority of grains are in the range of 400 – 500 nm, whereas the average grain size is found to be 450 nm which is supported by SEM analysis. Figure 5.7d shows peak distribution curve for grain roughness of BHNF ceramic [Gautam *et al.* (2016)].

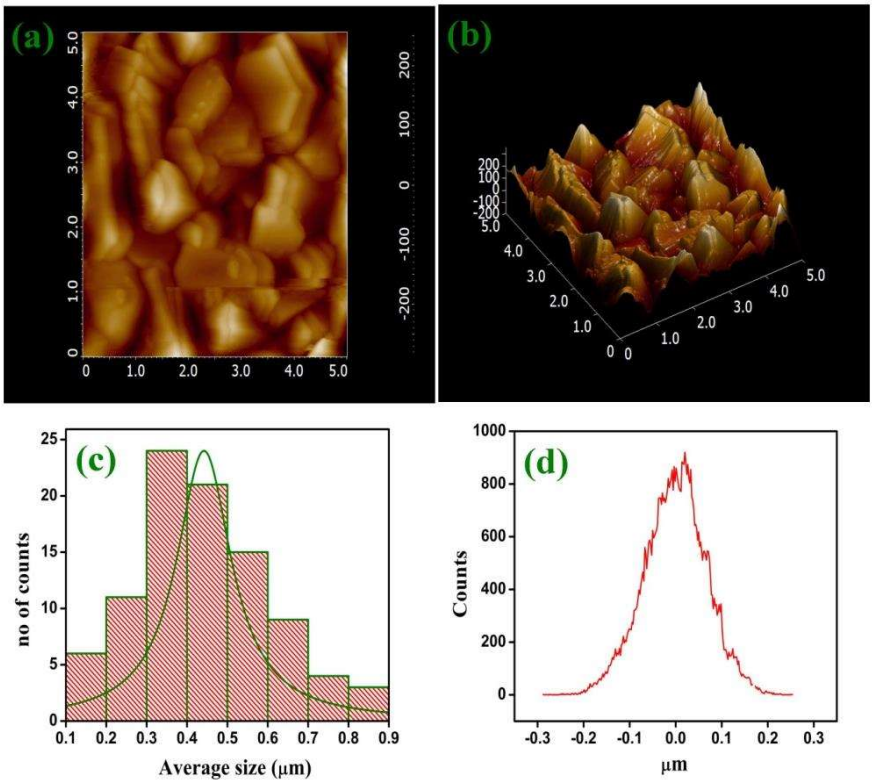

Figure 5.7 AFM images of BHNF ceramic at compositions x = 0.2 **(a)** two dimensional image for grain boundary (**b)** three dimensional for surface roughness (**c)** depth histogram graph and (**d)** bar diagram for particle size distribution.

5.4. Ferroelectric Properties

Ferroelectric behavior of nickel doped barium hexaferrite ($BaFe_{12-x}Ni_xO_{19}$, where x= 0.0, 0.05, 0.1 and 0.2) ceramic was investigated by polarization versus electric field (P-E) hysteresis curve, shown in Figure 5.8. The measurement of polarization of BHNF ceramic were observed with the help of PE loop tracer at the room temperature and 100 Hz frequency with corresponding electric field 5 kV/cm.

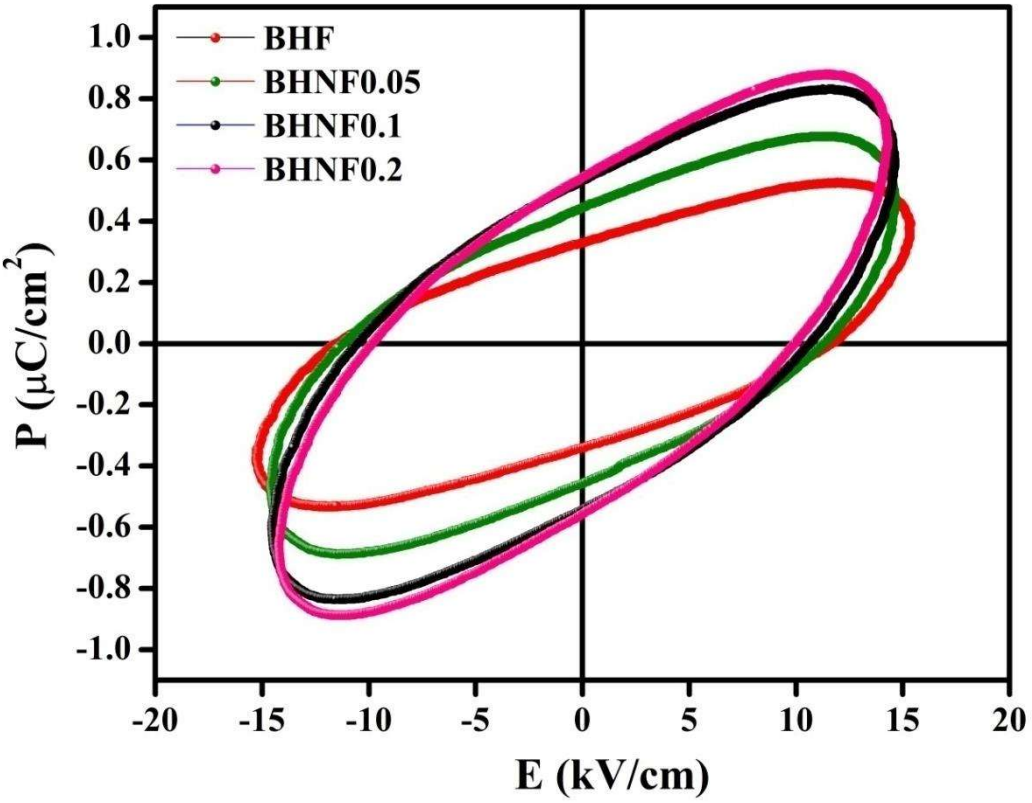

Figure 5.8 indicates P-E hysteresis loop for the compositions (x = 0.0, 0.05, 0.1 and 0.2) for BHNF ceramic.

It is observed from the figure, the value of remnant polarization (P_r) parallel increases with increasing amount of Ni^{+2} concentration, however coercivity (E_c) value decreases with Ni^{+2}

concentration. The value of remnant polarization and coercivity calculated from the graph for few selected Ni concentration at room temperature and listed in the table 5.2. It is observed from the table that the value of Pr for BHNF ceramic with compositions x = 0.2 was observed to be higher than the other compositions suggesting the enhancement of ferroelectric nature of this materials [Hoque *et al.* (2018)]. Furthermore, saturation polarization is not observed in P-E hysteresis loop for all selected compositions (x = 0.0, 0.05, 0.1, 0.2) which explained lossy capacitor nature of the BHNF ceramic because of combined effect of parallel joined capacitor and resistor.

Table 5.2 Remnant polarization (P_r) and Coercivity (E_c) of BHNF(x = 0.0, 0.05, 0.1 and 0.2) ceramic at room temperature.

compositions (x)	Remnant polarization ($\mu C/cm^2$)	Coercivity (kV/cm)
BHF	0.331	11.731
BHNF0.05	0.439	11.307
BHNF0.1	0.531	10.708
BHNF0.2	0.537	9.956

5.5. Magnetic studies

Figure 5.9 represents the M–H hysteresis loop of BHNF ceramic with compositions x = 0.0, 0.05, 0.1 and 0.2 at 100 K recorded at ±2 T. The saturation magnetization (M_s) and remnant magnetization (M_r) decreases with increasing concentration. This inverse behavior of magnetization with concentration is due to the existence of spin canting and superexchange interaction of Fe^{3+}–O^{2-}–Fe^{3+} on the substitution of Ni^{+2} ions in $BaFe_{12}O_{19}$ ceramic [Liu *et al.* (2002)]. The lower values of coercivity (H_c) of the BHNF ceramic as compared to barium

hexaferrite is due to the presence of unsymmetrical hexagonal particles as reported in earlier [Mallick *et al.* (2007)].

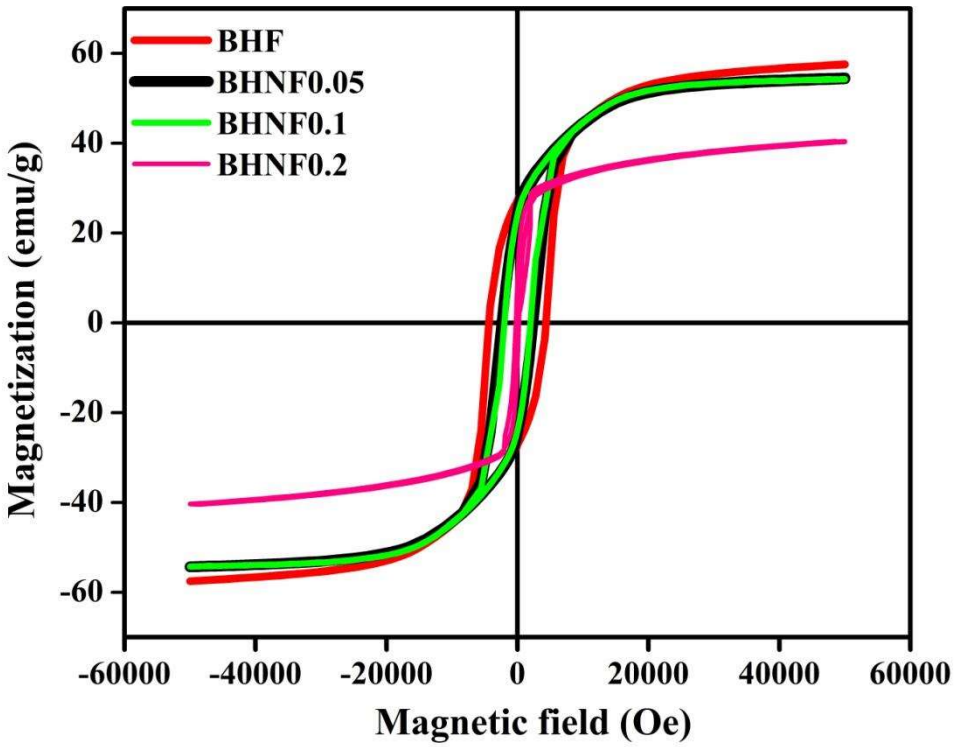

Figure 5.9 the variation of magnetization with magnetic field at 100 K temperature and different compositions of BHNF ceramic sintered at 1200 °C for 6 h.

The decrease in coercivity of nickel-doped barium hexaferrite may be attributed due to reduction in the rate of magnetocrystalline anisotropy field with increasing the concentration of Ni content [Waqar *et al.* (2018)]. This may lead to increasing the electrical properties such as conductivity of the materials which may be useful in sensor, transducers and catalysts. The squareness ratio (M_r/M_s) values for BHNF ceramic are near to 0.5 at room temperature. The lower value of M_r/M_s suggests that BHNF ceramic having a single domain, non interacting particles which are randomly oriented, exhibit hard magnetic properties [Mahmood *et al.*

(2014)]. The magnetic parameters such as saturation magnetization (M_s), remnant magnetization (M_r) and coercivity (H_c) for BHNF ceramic obtained from hysterias loop with different concentrations are mentioned in the table 5.3.

Table 5.3 Magnetic parameters of $BaFe_{12-x}Ni_xO_{19}$ ceramic with x = 0.0, 0.05, 0.1 and 0.2 compositions.

Parameters	BHF	BHNF0.05	BHN0.1F	BHN0.2F
M_s (emu/g)	54.19	50.18	49.82	36.79
M_r (emu/g)	27.25	25.04	24.00	16.34
Hc (A/m)	3.56×10^5	1.81×10^5	1.72×10^5	4.37×10^4
$S_q = M_r/Ms$	0.502	0.49	0.482	0.44

5.6. Dielectric studies

The dielectric constant and dielectric loss of BHNF ceramic having composition x = 0.0, 0.05, 0.1 and 0.2 as a function of temperature at 10 kHz is shown in Figure 5.10a and b. It is observed from the figure that both of dielectric constant and dielectric loss value increases with increasing concentration of nickel in the BHNF ceramic. The value of ε and tan δ at constant frequency (10 kHz) obtained from the plots are found to be 224 and 0.35, respectively of nickel doped barium hexaferrite (BHNF) ceramic. The increase in ε value with Ni doping can be attributed to the hopping of electrons between Fe^{2+} and Fe^{3+} and the hole transfer between Ni^{3+} and Ni^{2+} ions which invoke the contribution towards polarization mechanism. By the addition of divalent Ni ions, the exchange interaction between Ni^{2+} and Fe^{3+} may become possible resulting in the conversion of Fe^{3+} into Fe^{2+} and Ni^{2+} into Ni^{3+} ions.

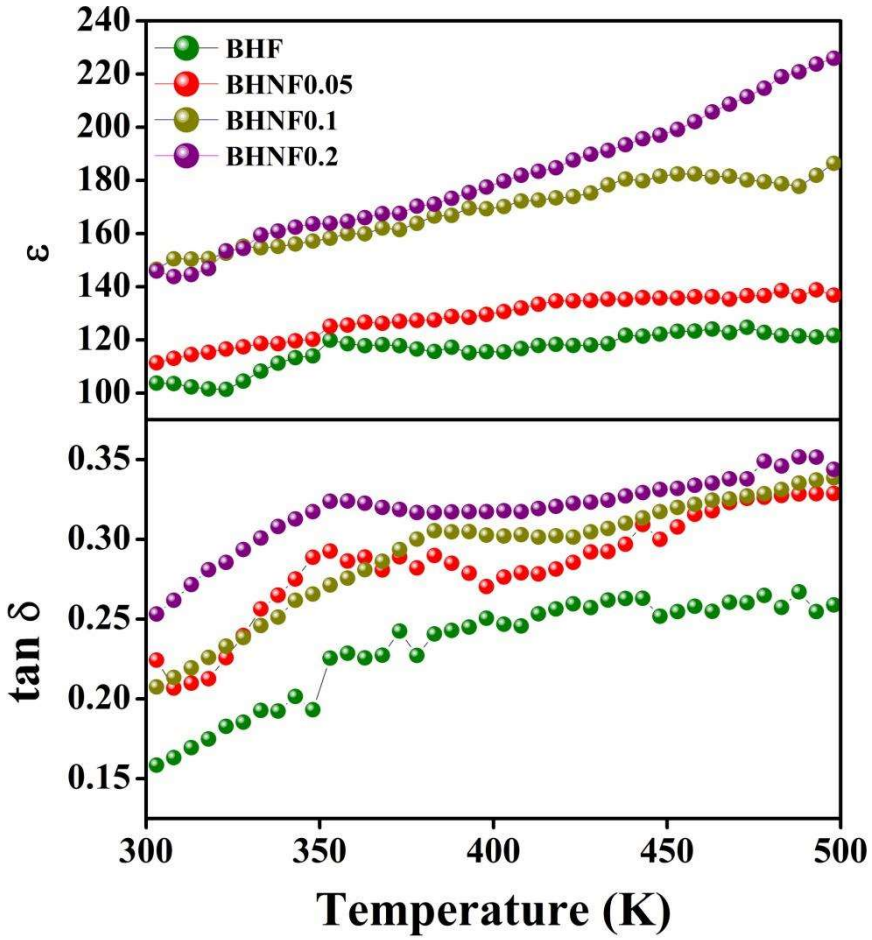

Figure 5.10 The dielectric constant and dielectric loss of BHNF ceramic with the composition x = 0.0, 0.05, 0.1 and 0.2 as a function of temperature at 10 kHz.

This interaction might contribute to the increase in electron/hole hopping between Fe^{3+} and Fe^{2+} as well as between Ni^{3+} and Ni^{2+} ions which in turn increases the piling up of electrons at the grain boundary [Iqbal and Farooq (2010)].

The effect of frequency on the dielectric constant (ε) and dielectric loss (tan δ) with the concentration x= 0.0, 0.05, 0.1 and 0.2 is shown in Figure 5.11. It is observed from Figure 5.11a

that the value of dielectric constant decreases with increasing frequency and is almost constant towards higher frequency, due to reversibility of electric field which takes place so rapidly.

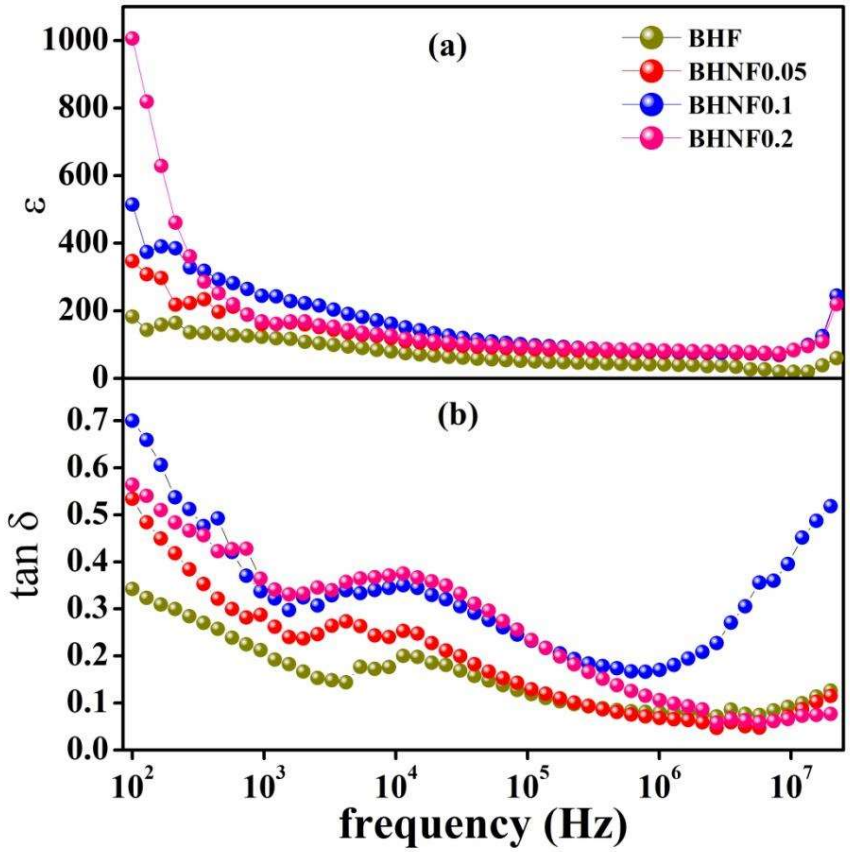

Figure 5.11 Frequency dependence of dielectric constant and dielectric loss at 343 K and with the various compositions of BHNF ceramic sintered at 1200 °C for 6 h.

The value of ε is found to be 1000 at 343 K and 100 Hz. The higher value of dielectric constant at lower frequency may be due to the interfacial charge polarization between semiconducting grains as well as insulating grain boundaries which is supported by internal barrier layer capacitance (IBLC) mechanism [Bueno (2007), Singh *et al.* (2014), Singh *et al.* (2015), Khare *et al.* (2014)]. The variation of dielectric loss (tan δ) with frequency of BHNF

ceramic with composition x= 0.0, 0.05, 0.1 and 0.2 is shown in Figure 5.11b. The values of tan δ increases with increase of concentration (varies in between 0.3 to 0.7) and are almost independent in higher frequency. Further decrease in dielectric loss was observed with the increase in frequency. This decrease can be due to the fact that the dipole oscillations cannot follow the changes of the external electric field at high frequencies [Soman *et al.* (2014), Sharma *et al.* (2014), Kannan *et al.* (2017), Yadava *et al.* (2017)].

5.7. Conductivity measurements

The plots of AC conductivity versus frequency at few selected compositions at 303 K temperature are shown in Figure 5.12 to understand conduction mechanism of BHNF ceramic. It is revealed that the conductivity remains unchanged up to the certain frequency after which it linearly increases with the frequency. The total conductivity of the materials can be calculated with the help of Almond–West type power law as per Eq. 5.2 and frequency dependent part of conductivity is measured by Jonscher's power law expressed as the following Eq. 5.3.

$$\sigma = \sigma_{dc} + \sigma_{ac} = \sigma_{dc} + A\omega^{s} \tag{5.2}$$

$$\sigma_{ac} = A\omega^{S} \tag{5.3}$$

where, the first term of the Eq. 5.2 corresponding to DC conductivity due to free charge carriers and the last term corresponding with AC conductivity of the materials that explain the hopping charge mechanism. A indicates temperature dependent pre-exponential factors measures the strength of the polarizability. The parameter s is dimensionless exponent term s (0 < s < 1) and strongly dependent on the temperature as well as compositions of the materials and measures

polarization mechanism in between the lattices around them and the mobile ions [Mandal *et al.* (2017)].

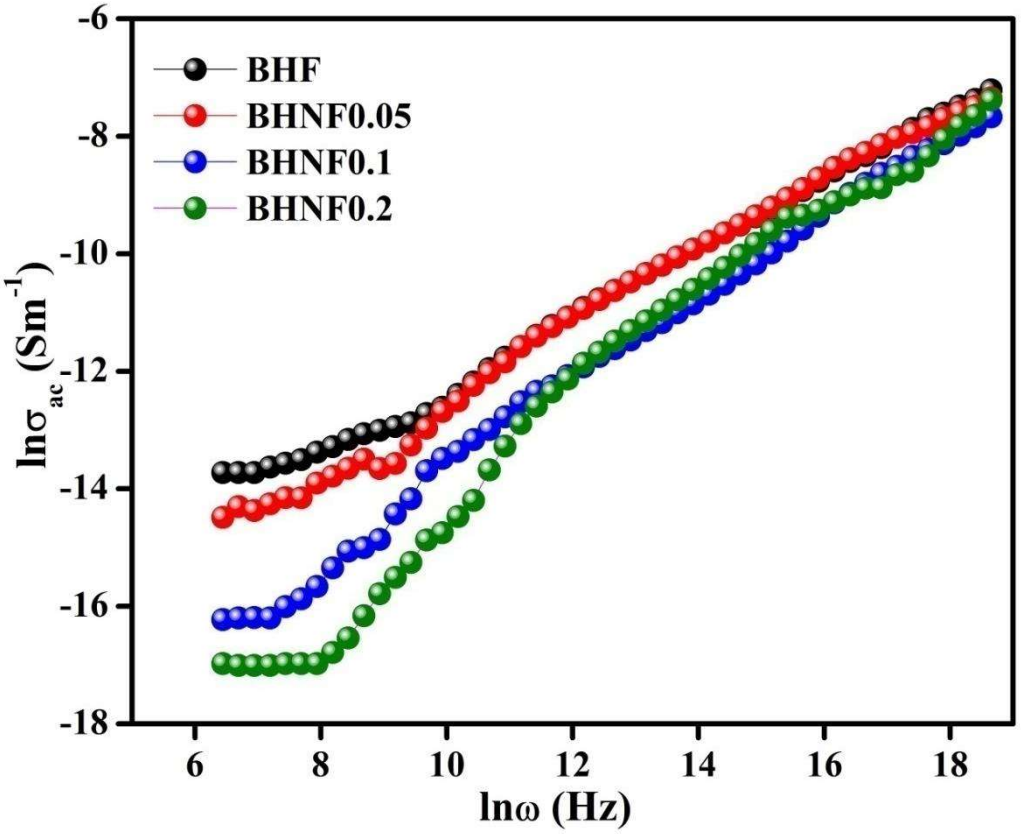

Figure 5.12 plots of AC conductivity versus frequency at few selected compositions at 303 K temperature.

The value of s for BHNF ceramic calculated from the plot and found to be 0.467, 0.473 0.559 and 0.926, respectively with the composition (Ni^{2+} = 0.0, 0.05, 0.1, and 0.2) at 343 K temperature. The observed value of s from the plots for given concentrations are approximately equal to one. It is observed that the value of exponent parameter obtained by linear square fitting increases with increasing Ni^{+2} concentration enhances the conductivity due to the possible

electron transfer between Fe^{2+} and Fe^{3+} ions and the hole transfer between Ni^{2+} and Ni^{3+} ions related to the hopping charge conduction mechanism in the BHNF ceramic [Macdonald and Johnson (2005)]

The plot of ln σ vs. 10^3/T of BHNF ceramic with the composition x = 0.0, 0.05, 0.1 and 0.2, at 100 Hz are depicts in Figure 5.13 reveals increasing in conductivity with the temperature.

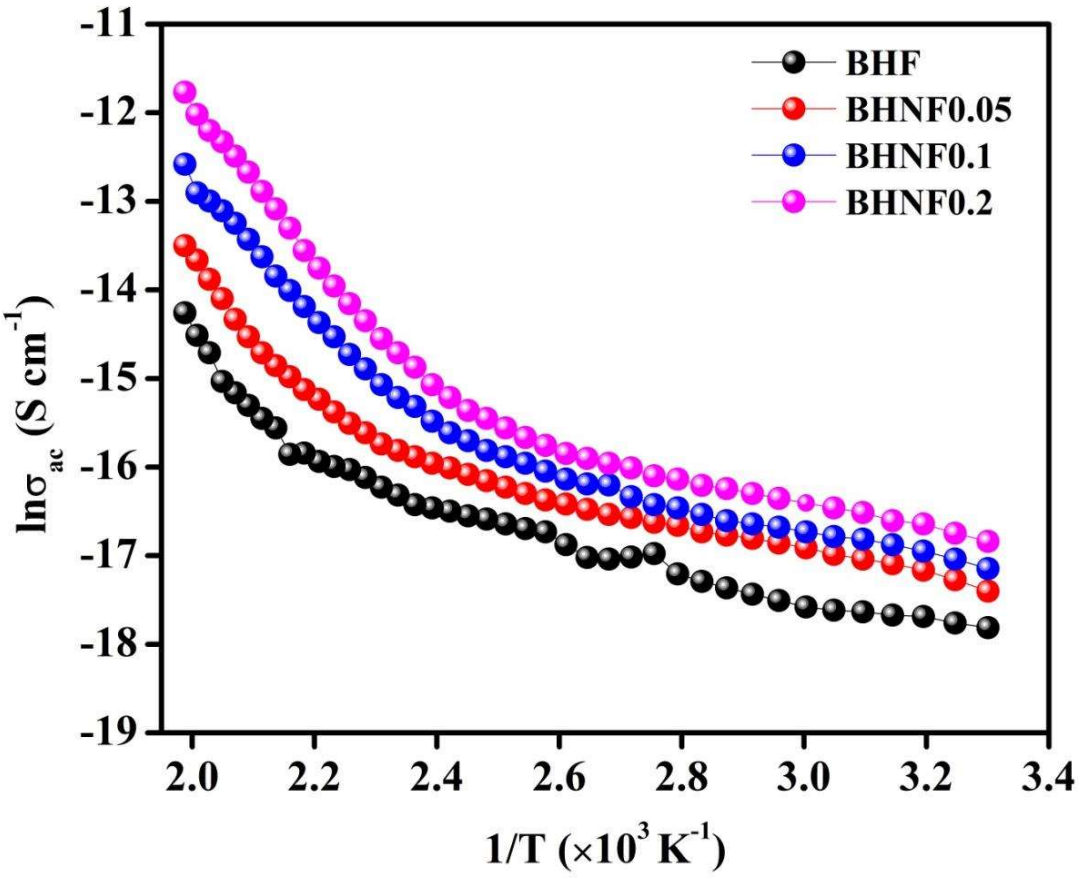

Figure 5.13 plots of ln σ vs. 10^3/T of BHNF ceramic with the composition x = 0.0, 0.05, 0.1 and 0.2, at 100 Hz and certain concentrations.

Electrical conduction observed in the materials with the temperature variation due to both of hopping charge carriers and transportation of charge via excited state followed by the Arrhenius law, can be expressed as the following Eq. 5.4.

$$\sigma = \sigma_0 \exp(\frac{-E_a}{kT}) \quad (5.4)$$

where, σ_0 is the pre-exponential factor, E_a is the activation energy for electrical conduction in the materials, T is the absolute temperature and k is the Boltzmann constant. The activation energy of BHNF ceramic is calculated with the help of the slope of the curves were found to 0.76, 1.34, 1.37 and 1.52 eV for the compositions x = 0.0, 0.05, 0.1 and 0.2, respectively at higher temperature regions. The increase in the value of activation energy (Ea) with increases in concentration may be due to hopping charge mechanism between $Fe^{2+} \leftrightarrow Fe^{3+}$ and $Ni^{3+} \leftrightarrow Fe^{2+}$ in the octahedral sites that is responsible for increase of electrical conduction of the synthesized materials [Gul and Maqsood (2008), Gul *et al.* (2010), Samad *et al.* (2019)].

5.8. Impedance studies

The contribution due to grain, grain boundary and electrode effect in the ceramic materials were understood with the help of impedance spectroscopy studies. The presence of grain, grain boundary and electrode effect in the materials were represented by the semicircular arcs. The semicircular arcs at lower, middle and at higher frequency region are due to electrode, grain boundary, and grain contributions, respectively. The impedance plane plots of imaginary (Z″) versus real (Z′) of BHNF ceramic with the compositions x = 0.0, 0.05, 0.1 and 0.2 at the room temperature are shown in the Figure 5.14 (a) and (b). The presence of only one semi-circular arcs for each compositions is observed in Figure 5.14 (a) due to large difference in the resistance of

grains and grain boundaries. On zoom view at higher frequency region (Figure 5.14 (b)), two semicircular arcs at middle and higher frequency region were observed in the materials which may be due to grain boundaries and grain contribution.

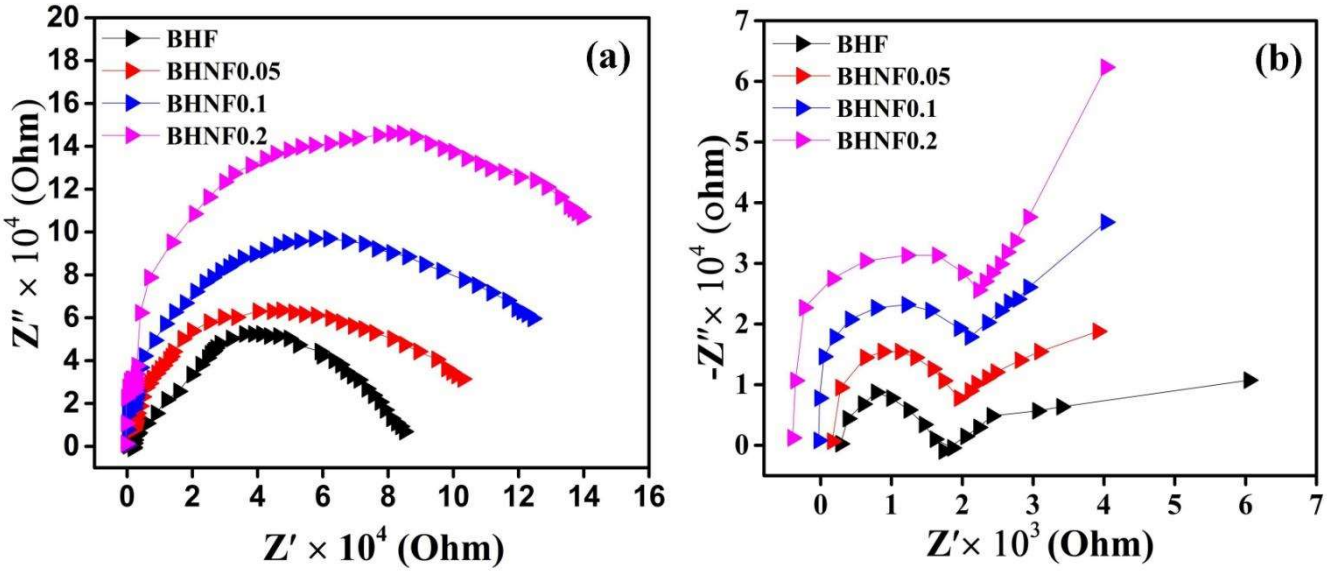

Figure 5.14 Impedance plane plots of Z′ vs Z″ of $BaFe_{12-x}Ni_xO_{19}$ with the compositions x = 0.0, 0.05, 0.1, and 0.2 (a) grain boundaries at low frequency (b) grain at low frequency.

The impedance of grain and grain boundary can be calculated by the following Eq. 5.5

$$Z^* = \frac{1}{R_g^{-1} + i\omega C_g} + \frac{1}{R_{gb}^{-1} + i\omega C_{gb}} = Z' - iZ'' \qquad (5.5)$$

Where $Z' = \frac{R_g}{1+(\omega R_g C_g)^2} + \frac{R_{gb}}{1+(\omega R_{gb} C_{gb})^2}$

And $Z'' = R_g \left[\frac{\omega R_g C_g}{1+(\omega R_g C_g)^2}\right] + R_{gb} \left[\frac{\omega R_{gb} C_{gb}}{1+(\omega R_{gb} C_{gb})^2}\right]$

where Z*, Z′, and Z″ are the complex, real, and imaginary impedance, R_g and R_{gb} represent the resistance of the grain and grain boundary, C_g and C_{gb} indicate the capacitance of the grain and grain boundary, and ω represents the angular frequency. The resistance of grain (R_g) and grain boundary (R_{gb}) of BHNF ceramic were calculated with the help of semicircular arc which are mentioned in the table 5.4. The larger difference observed in between the resistance of grain and grain boundaries clearly indicates the semiconducting grains with the insulating grain boundaries which was supported by internal barrier layer capacitance (IBLC) mechanism [Barbier *et al.* (2012)].

Table 5.4 Calculated value of grain and grain boundary resistance and their conductivity at few selected compositions of BHNF Ceramic.

Compositions	**R_g (ohm)**	**R_{gb} (ohm)**	**C_g (pF)**	**C_{gb} (pF)**
BHF	1738.215	85006.87	9.66	0.0128
BHNF0.05	1954.233	102874.12	0.11	0.0224
BHNF0.1	2108.009	124366.13	0.168	0.0305
BHNF0.2	2228.832	139450.80	0.124	0.0129

5.9. Conclusion

BHNF ceramic nanostructure materials with the compositions x= 0.0, 0.05, 0.01 and 0.2 have been successfully synthesized by a chemical route. X- ray diffraction pattern confirmed the hexagonal phase formation of BHNF ceramic at 1200 °C for 6 h. The hexagonal structure of the

particle were confirmed by TEM analysis and size of the particles were observed with the help of Image J software and found to be 332, 221, and 120 nm on the scale 200 nm for the composition x = 0.0, 0.05 and 0.1, respectively, however particle size was found to be 16 nm on the scale of 50 nm for the composition x = 0.2 of BHNF ceramic. The value of dielectric constant (ε') is found to be 1000 at 343 K and 10 kHz. The higher value of dielectric constant for the materials was explained on the basis of impedance plane plots which showed the semiconducting grain with the insulating grain boundaries. The squareness ratio (M_r/M_s) values for all compositions of BHNF ceramic were observed near to 0.5 at room temperature. The lower value of squareness (M_r/M_s) ratio indicates the presence of mono domain crystal structure, justifies its suitability in various applications such as high magnetic recording media and permanent magnet.